Enhanced Electrical Switching and Electrochromic Properties of Poly(p-phenylenebenzobisthiazole) Thin Films Embedded with Nano-WO3

ARTICLE *in* ADVANCED FUNCTIONAL MATERIALS · SEPTEMBER 2010

Impact Factor: 11.81 · DOI: 10.1002/adfm.201000261

6 AUTHORS, INCLUDING:

Jiahua Zhu
University of Akron
131 PUBLICATIONS **2,554** CITATIONS
SEE PROFILE

Suying Wei
Lamar University
228 PUBLICATIONS **4,482** CITATIONS
SEE PROFILE

Zhanhu Guo
University of Tennessee
367 PUBLICATIONS **6,388** CITATIONS
SEE PROFILE

ADVANCED FUNCTIONAL MATERIALS
www.afm-journal.de

Enhanced Electrical Switching and Electrochromic Properties of Poly(p-phenylenebenzobisthiazole) Thin Films Embedded with Nano-WO_3

By *Jiahua Zhu, Suying Wei,* Max Jr. Alexander, Thuy D. Dang, Thomas C. Ho,* and *Zhanhu Guo**

The electrical switching and electrochromic phenomena of a novel nanocomposite comprising poly(p-phenylenebenzobisthiazole) (PBZT) and tungsten oxide (WO_3) nanoparticles are investigated as a function of the nanoparticle loading. Both dissolving PBZT and doping PBZT backbone structure with acid are achieved by one simple step. Chlorosulfonic acid (CSA) is used as a solvent and spontaneously transformed to sulfuric acid upon exposure to moisture. The formed sulfuric acid serves as doping agent to improve the electrical conductivity of PBZT. The most significant enhancement of electrical switching is observed in the nanocomposites with low weight fraction (5%). The electrical conductivity of 5% WO_3/PBZT nanocomposite thin film is increased by about 200 times and 2 times, respectively, as compared to those of the as-received PBZT and PBZT/CSA thin films. As the nanoparticle loading increases to 20% and 30%, the nanocomposites follow an ohmic conduction mechanism. Stable electrical conductivity switching is observed before and after applying a bias on the pristine PBZT and WO_3/PBZT nanocomposite thin films. Electrochromic phenomena of both PBZT and WO_3/PBZT nanocomposite thin films with high contrast ratio are observed after applying a bias (3 V). The mechanisms of the nanoparticles in enhancing the electrical switching and electrochromic properties are proposed.

1. Introduction

Promising conjugated polymers have motivated considerable investigation as advanced materials for their various applications, such as photovoltaic cells,[1] electrochromic devices,[2] organic light-emitting diodes,[3] and fluorescence-based DNA detection.[4] Among the conjugated polymers, derivatives of poly(thiophene), poly(pyrrole), and poly(aniline) (PANI) are widely studied.[5] Numerous synthetic strategies have been developed to tune the physical properties of conjugated polymers[6] by tailoring the molecular structure of either the main chain or the pendant groups. Copolymerization of distinct monomers introduces the modification of the main chain structure and allows for combining the unique properties of each monomer.[7] An alternative functional group substitution of the parent hetero-cycle is used to change the physical and chemical properties through the induced steric or electronic effects.[8] Many other approaches to manipulate the physicochemical properties of conjugated polymers are reported through the formation of the blends,[9] laminates,[10] or composites.[11,12]

Polymer nanocomposites (PNCs), a special class of functional materials with unique physical, chemical and biological properties, originate from a suitable combination of nanoparticles and polymers. The electrochromism of WO_3,[13] magnetic susceptibility of γ-Fe_2O_3,[14–16] electrical conductivity of Au[17] and Ag nanoparticles,[18–20] optical properties of ZnO quantum dots,[21] and other physical properties have been successfully introduced to the PNCs. The nanomaterials have attracted much interest in both academic and industrial fields due to their unique physicochemical properties far beyond the simple addition of the advantages of each component. Therefore, combining their easy processability, light-weight and low-cost, PNCs have been extensively investigated for their potential wide applications.

Heterocyclic rigid-rod conjugated polymers have attracted considerable interest owning to their high mechanical strength, high modulus, and excellent thermal and environmental stability.[22,23] Poly(p-phenylene benzobisthiazole) (PBZT) is a member of rigid-rod conjugated polymers. The conjugated

[*] J. Zhu, Prof. T. C. Ho, Prof. Z. Guo
Integrated composites laboratory (ICL)
Dan F Smith Department of Chemical Engineering
Lamar University, Beaumont
TX 77710 (USA)
E-mail: zhanhu.guo@lamar.edu

Prof. S. Wei
Department of Chemistry and Physics, Lamar University
Beaumont, TX 77710 (USA)
E-mail: suying.wei@lamar.edu

Dr. M. Jr. Alexander, Dr. T. D. Dang
Electromagnetic Hardened Materials
Materials and Manufacturing Directorate
Air Force Research Laboratory
Wright-Patterson, AFB, OH 45433-7750 (USA)

DOI: 10.1002/adfm.201000261

benzothiazole and phenyl rings in the polymer backbone result in an extended delocalization of π electrons. Therefore, special electrical and optical properties derived from these materials are greatly anticipated, especially the electric and electrochromic properties. Electrochromism is broadly defined as a reversible optical change in a material induced by an external voltage, which has been found in both inorganic materials such as WO_3, V_2O_5, MoO_3 and $Ir(OH)_3$[24,25] and organic materials such as poly(3,4-propylenedioxypyrrole) (PProDOP),[2] poly(3,4-alkylenedioxythiophene) (PXDOT)[26] and poly(alkyl-3,4-ethylenedioxyselenophene) (PEDOS-Cn) with tunable contrast ratio and coloration efficiency.[27] Among these, conjugated polymers have attracted considerable interest owning to their tremendous advantages, such as their ease processability, rapid response times, high optical contrasts, and the ability to modify their structure to create multicolor electrochromes.[2] Some works have reported on the electrochromic properties of conjugated polymer nanocomposites. For example, an enhanced transmittance of ~45% at 600 nm was reported on derivatized poly(pyrrole)/WO_3 nanocomposites.[28] Recently, Jia et al. found that the electrochromic contrast and switching time of POSS-poly(aniline)/poly(2-acrylamido-methane-2-propanesulfonic acid) (POSS-PANI/PAMPS)$_{50}$ is increased by more than 30% and significantly shorter than those of (PANI/PAMPS)$_{50}$, respectively.[29] However, the electrical switching and electrochromism of the rigid-rod PBZT nanocomposites is less investigated.

In this work, high quality WO_3/PBZT nanocomposite thin films are successfully fabricated with a simple one-step method. Chlorosulfuric acid (CSA), as a solvent for dissolving PBZT, is transformed to the doping acid during the formation of thin films. Both the electrical switching and electrochromic properties are investigated on the resulting thin films. The synergistic interaction between the semiconductive nanoparticles and conductive polymer is indicated by the UV-vis absorption and is responsible for the observed improved electrical switching and electrochromic properties in the WO_3/PBZT nanocomposite thin films. The stable enlarged improvement of electrical conductivity for nanocomposite thin films is observed with an applied external voltage. The mechanisms of the enhanced electrical switching and electrochromic properties are proposed in this work.

2. Results and Discussion

2.1. FT-IR Analysis

Figure 1 shows the FT-IR spectra of the pristine PBZT and WO_3/PBZT nanocomposite thin films casted from CSA solution after exposure to air for 24 h. The molecular structure of PBZT is shown in **Scheme 1**. For comparison, the spectrum of WO_3 nanoparticles is also shown in Figure 1. Neither a new band nor band shift is observed after incorporating the WO_3 nanoparticles in the PBZT thin film, indicating that the composition of PBZT is not changed after dissolving in CSA and adding the nanoparticles. However, the nanoparticles have intensified the major bands at around 800–1200, 1600–1800 and 3392 cm^{-1}. The band at 872 cm^{-1} is assigned to the S–O stretching. The strong bands at 1028 cm^{-1} and 1167 cm^{-1} are attributed to the RO–SO_3^- stretching. The intensity of band at 1028 cm^{-1} relatively

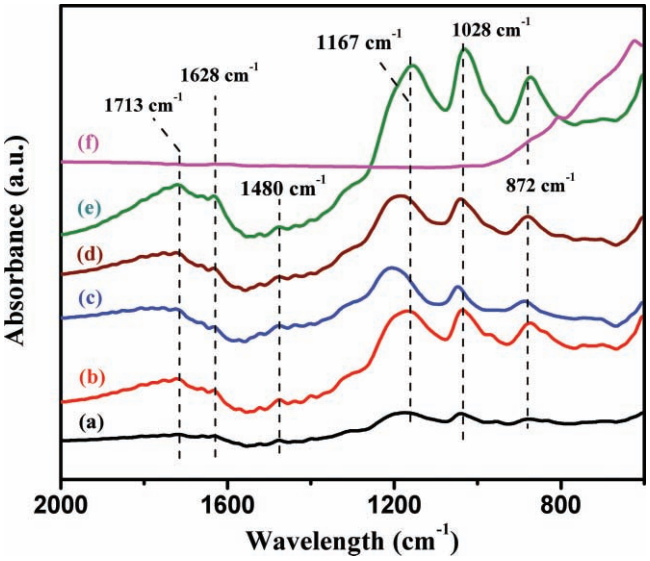

Figure 1. FT-IR spectra of a) pristine PBZT, and PBZT nanocomposite thin films with WO_3 nanoparticle loading of b) 5 wt%, c) 10 wt%, d) 20 wt%, e) 30 wt%, and f) 100 wt%.

increases with the increase of the WO_3 nanoparticle loading and is even higher than that of the band at 1167 cm^{-1} in the WO_3/PBZT nanocomposites with a loading of 30 wt%. This observation indicates a slight polarity change of the sulfuric acid group after forming the hydrogen bonding between sulfuric acid and PBZT backbone. Similar intensified bands for the S–C=N and N–H stretching are observed at 1628. The band at 1480 cm^{-1} represents the C=N stretching vibration.[30] No bands are observed at around 1410–1375 cm^{-1}, which corresponds to the characteristic bond of RSO_2–Cl, indicating that CSA has completely reacted with the moisture in the air.

2.2. Electrical Conductivity Switching Phenomenon

2.2.1. Without an Applied External Voltage

The electrical conductivity of the as-received PBZT and WO_3/PBZT nanocomposite thin films casted from CSA solution is studied using the standard four-probe measurement. **Figure 2** shows the current–voltage (I–V) curves obtained from these samples. The current doesn't change with the variation of the applied voltages for the as-received PBZT thin film, which indicates an almost non-conductive behavior. However, the PBZT and WO_3/PBZT nanocomposite thin films casted from the CSA solution show entirely different electrical behaviors from that of the as-received PBZT thin film. These casted films clearly display electrical switching phenomenon that behaves like a diode, in which the current is strongly dependent on the applied voltage. This electric characteristic is consistent with our prior results obtained from the as-received PBZT thin films through acid doping process.[31] In this case, the voltage-dependent (non-linear) current can be roughly divided into three stages, the first stage is from –1.0 V to –0.5 V, which represents the high electrical conductivity together with a transition to a

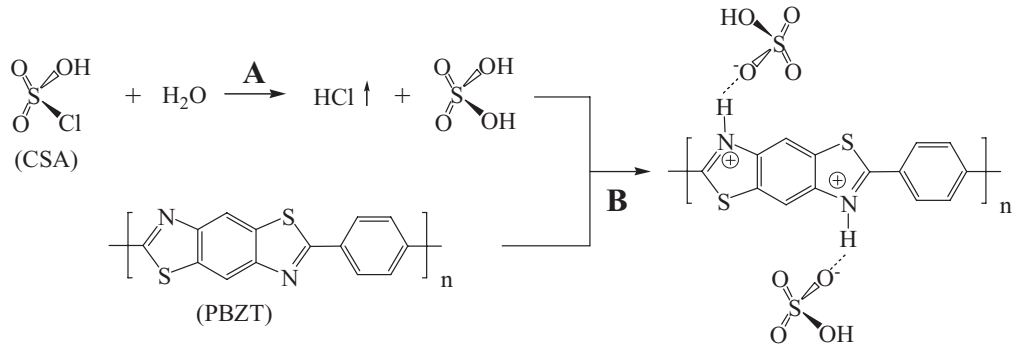

Scheme 1. A) Dissolution of CAS upon exposure to air, and B) its subsequent doping of PBZT.

lower conductivity; the second stage is from –0.5 V to 0.5 V, which reflects a lower conductivity from the linear *I–V* curve; the third stage is above 0.5 V, and the electrical conductivity switches to a higher value. The conductivity calculated from the *I–V* curves in each stage is summarized in **Table 1**. The conductivity of these samples varies following the sequence of stage (I) > stage (III) > stage (II). The conductivity of WO_3/PBZT nanocomposites thin film with 5% nanoparticle loading increases by about 200 times and 2 times, as compared to those of the as-received PBZT and PBZT/CSA thin films in the first stage, respectively. The electrical conductivity decreases gradually with the increase of the WO_3 nanoparticle loading. The conductivity of the nanocomposite films filled with 20% and 30% WO_3 nanoparticles is about half of the PBZT/CSA thin film in the first stage. It is interesting to notice that these two films show linear electrical conduction behavior rather than a switching phenomenon. In the second stage, the lower conductivity is observed for the WO_3/PBZT nanocomposite thin films with a particle loading of 5% and 10% as compared to that of the casted PBZT/CSA film. WO_3/PBZT nanocomposite thin film with a nanoparticle loading of 5% still acquires the highest conductivity in the third stage, indicating the more efficient electrical switching behaviors.

The electrical behavior difference between the as-received PBZT and PBZT/CSA thin films is attributed to the proton doped backbone structure of the PBZT. After processed to the thin film, CSA tends to react with the moisture in air and forms sulfuric acid within the PBZT film. The reaction between CSA and moisture is shown in Scheme 1A.

The acid doping mechanisms for the enhanced electrical conductivity are proposed in our prior work.[31] In the present study, CSA is used to dissolve PBZT and more importantly, the formed sulfuric acid dopes PBZT to render it electrically conductive. For the WO_3/PBZT nanocomposite thin films, interfacial interaction between the nanoparticles and polymer plays a significant role in improving the electrical switching efficiency (higher ratio of $\sigma(I)/\sigma(II)$) when the particle loading is relatively low, like 5 wt% and 10 wt%. The WO_3 nanoparticles serve as charge transfer centers between the polymer chains, which greatly enhance the polymeric chain-chain charge transfer and thus promote the interchain electron transfer efficiency. Meanwhile, the electron pairs of oxygen in the sulfate group absorbed on the particle surface form hydrogen bonding with the protonated polymer chains and thus result in a decreased polymeric interchain space, which leads to the reduced inter-chain resistance. Both factors contribute to the improved electrical conductivity in the WO_3/PBZT nanocomposite thin films in the first stage. However, as the particle loading further increases to 20 wt% and 30 wt%, the *I–V* curves show almost linear characteristic,

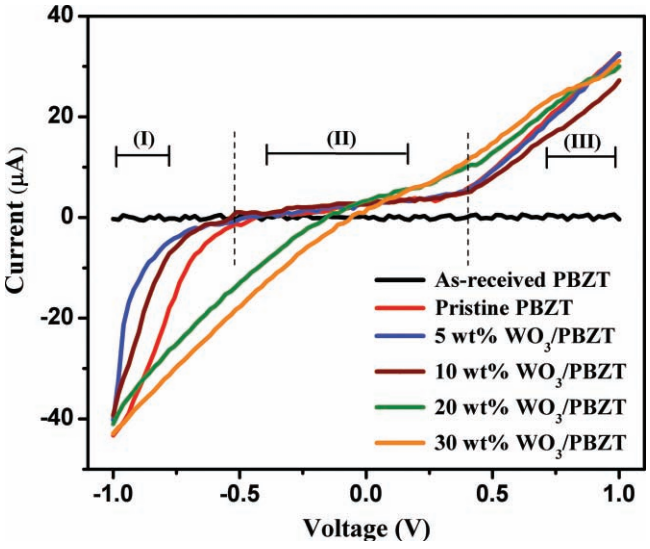

Figure 2. The *I–V* curves for the as-received PBZT and WO_3/PBZT nanocomposite thin films casted from CSA solutions.

Table 1. The electrical conductivity under varied sweeping voltages for the as-received PBZT thin film and the WO_3/PBZT nanocomposite thin films casted from CSA solutions.

Composition	Electrical conductivity [σ, mS cm^{-1}]		
	Stage (I)	Stage (II)	Stage (III)
As-received PBZT	0.10	0.10	0.10
PBZT/CSA	5.23	0.29	2.03
5% WO_3/PBZT/CSA	15.45	0.24	2.06
10% WO_3/PBZT/CSA	7.22	0.19	1.64
20% WO_3/PBZT/CSA	2.18	0.67	1.57
30% WO_3/PBZT/CSA	2.14	1.19	1.56

indicating the disappearance of the electrical switching phenomenon. This significant change arises from the reduced distance between the nanoparticles as the loading increases, and the main pathway for the electron transport switches from polymer chain to particle-particle tunneling, which is also consistent with the recent work of particle connectivity for a conductive polymer.[32] In the particle connectivity conductive polymer mechanism, Yoo et al.[32] have found that the macroscopic conductivity of polymer scales linearly with the particle density, especially the packing of these particles which governs the macroscopic conductivity in the solid state. Electrical switching is also observed in the silver/polyaniline nanocomposites, and Oliveira et al. explain the switching conductivity in terms of the charge transfer between the polymer and Ag nanoparticles, which is strongly influenced by the interface between these two components.[20]

2.2.2. With an Applied External Voltage

The pristine PBZT and WO_3/PBZT nanocomposite thin films show not only the electrical conductivity switching induced by the intrinsic structure change under different sweeping voltages,[31] but also the electrical conductivity switching stimulated by an applied external electrical potential (**Figure 3**). Figure 3 shows the electrical conductivity change of the thin films with and without an applied external potential of 3 V. All the thin films are observed to have excellent electrical on-off switching properties, and perform good switching stability and repeatability. The V-off conductivity is observed to increase slightly after the thin films experience the first V-on cycle and then both the V-off and V-on conductivities are stabilized at the same level in the later on-off cycles. The increased conductivity after applying voltage implies that the applied bias alters the local surface potential enough to change the oxidation state of the molecule,[33] which is revealed by the UV-Vis spectroscopy in **Figure 4**. In the perspective of electron transfer, the localized electrons on the identifiable molecular sites are transported under the impetus of concentration gradients by a self-exchange process among the occupied and unoccupied electron sites and thus enhance the electrical conductivity by the accelerated electron movement.[34] Once the external potential is removed, the electron concentration gradient disappears suddenly and only small amount of localized electrons in the PBZT backbone structure exist in the film, thus the conductivity is sharply decreased, however it is still higher than that of the as-prepared thin films owning to the residual electrons.

A slight decrease in the V-on conductivity is observed after several scans, which was also observed in other polymer systems owning to the degradation.[35,36] However, the conductivity switching response is well maintained, indicating that these materials possess good cycling stability and can be switched between the V-on and V-off states many times without degradation.

The addition of WO_3 nanoparticles in the thin film greatly increases the switching efficiency, which is demonstrated by the conductivity improvement [conductivity improvement = $(V_{on} - V_{off})/V_{off}$]. When the particle loading is 5 wt%, the highest conductivity improvement of around 133% is observed, and followed by 51%, 40%, and 40% for WO_3/PBZT nanocomposite thin films with a particle loading of 10 wt%, 20 wt% and 30 wt%, respectively (**Figure 5**). These results correspond well to the conductivity change under varied sweeping voltages, and further

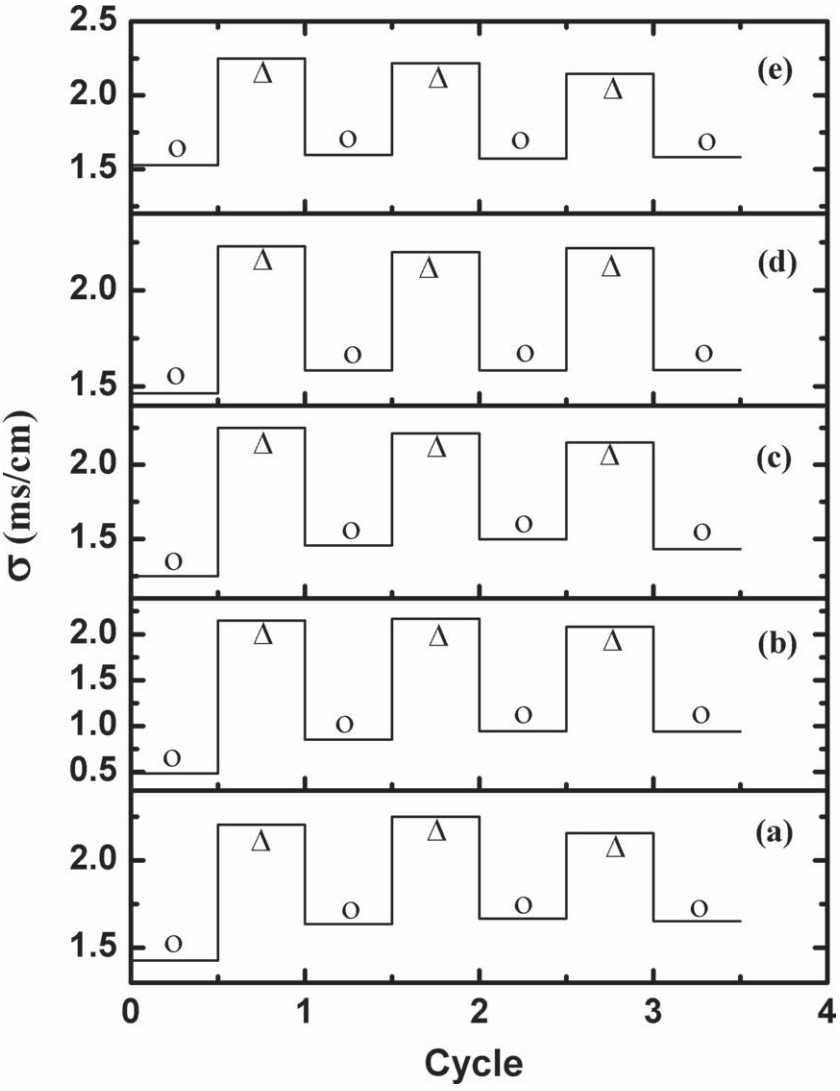

Figure 3. The cycles of the electrical switching properties under external potentials for a) pristine PBZT, and WO_3/PBZT nanocomposite thin films with a particle loading of b) 5 wt%, c) 10 wt%, d) 20 wt%, and e) 30 wt%. Δ indicates with a 3 V during the test; O means the voltage is removed during the test. The electrical conductivity is calculated from the voltage region of –0.5 ~ 0.5 V (linear region).

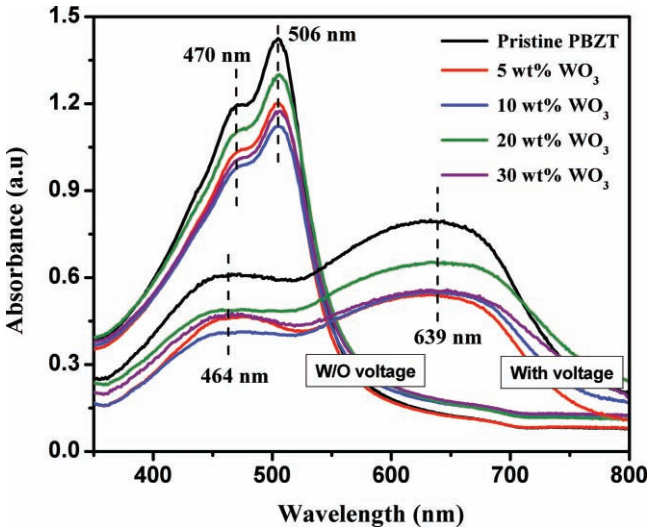

Figure 4. UV-Vis spectra of the pristine PBZT and WO_3/PBZT nanocomposite thin films with or without (W/O) applying voltage (3 V) during testing.

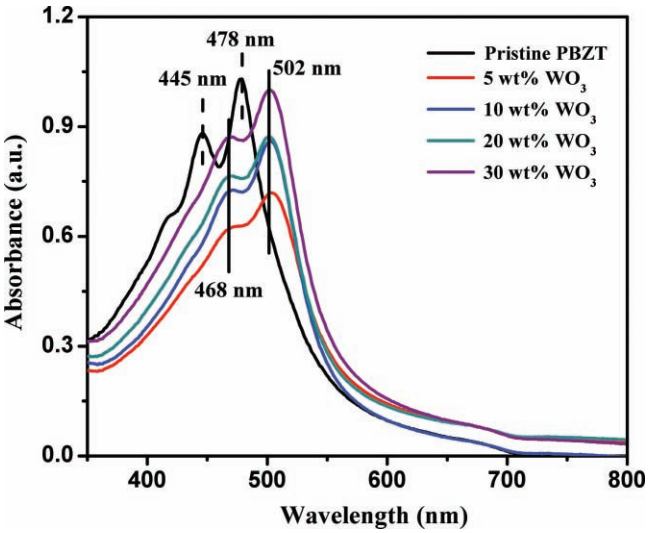

Figure 6. UV-Vis spectra of the pristine PBZT and WO_3/PBZT nanocomposite thin films after washing with DI water and drying in the vacuum oven overnight at 80 °C.

prove the significant effect of nanoparticles on the electrical conductivity in this system.

2.3. Optical Properties

2.3.1. UV-Vis Analysis

Figure 6 shows the optical absorption spectra of the pristine PBZT and WO_3/PBZT nanocomposite thin films with different particle loadings. The corresponding absorption peaks at 445 and 478 nm are observed for the pristine PBZT thin film. A significant red-shift of both peaks at 468 and 502 nm is observed for the WO_3/PBZT nanocomposites, which suggests that the electronic delocalization is increased in the nanocomposites. Similar red-shift is also observed in the 2,6-diphenylbenzo[1,2-d:4,5-d′]bisthiazole (t-DBZT)/$AlCl_3$ and t-DBZT/$GaCl_3$ complexes relative to the t-DBZT in dichloromethane.[37] Theoretical calculations prove the participation of the metal halide in the electron delocalization, which is responsible for the red-shift.[38] In this case, combining the semi-conductivity of WO_3 and the introduced hydrogen bonding between the polymer backbone and the nanoparticles, the electron delocalization is greatly enhanced and results in a higher electrical conductivity and more efficient switching behavior with a suitable content of the nanoparticles. The schematic electron transportation between polymer molecules is illustrated in **Figure 7**. However, as the nanoparticle loading increases to a higher value, such as 20 wt% and 30 wt%, the polymer-polymer interaction is greatly blocked and the particle-particle interaction becomes the dominating pathway for the electron transport, and thus the linear electrical conductivity is observed for the nanocomposite films at the loading of 20 wt% and 30 wt% (Figure 2.)

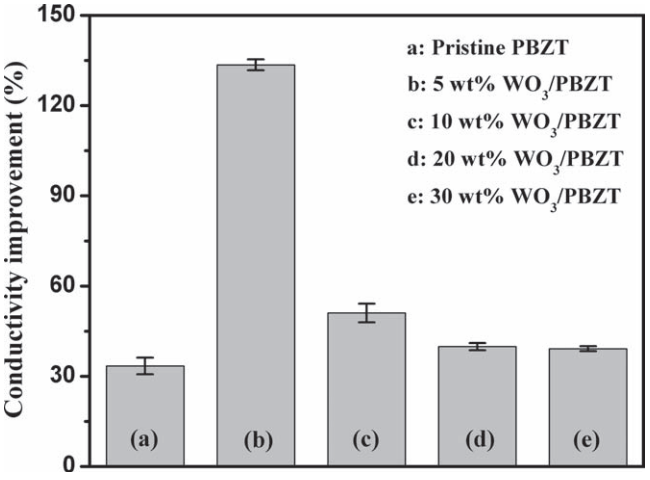

Figure 5. The electrical conductivity improvement for the PBZT/CSA and WO_3/PBZT nanocomposite thin films after applying 3 V potential.

2.3.2. Electrochromic (EC) Properties

PBZT has extremely high mechanical strength and thermal stability due to its rigid rod structure. However, the poor solubility limits its wider use due to the difficulties in processing PBZT into thin films or fibers. In this work, an easy one-step method to fabricate protonated PBZT and WO_3/PBZT nanocomposite thin films is introduced by using CSA as a solvent, which also serves as doping acid to protonate PBZT after exposing to moisture in air. To the best of our knowledge, few works have been reported on the electrochromic properties of PBZT, even fewer on the PBZT nanocomposites.

Figure 8 shows the color change of PBZT thin film before and after applying voltages. With a small voltage (3 V), the color of the thin film sharply changes from orange to dark blue within one second, and a quick color recovery is observed once the voltage is removed. The orange film represents the neutral state of PBZT and the dark blue is the reduced state. It is worth to notice that the film in both states shows high transparency.

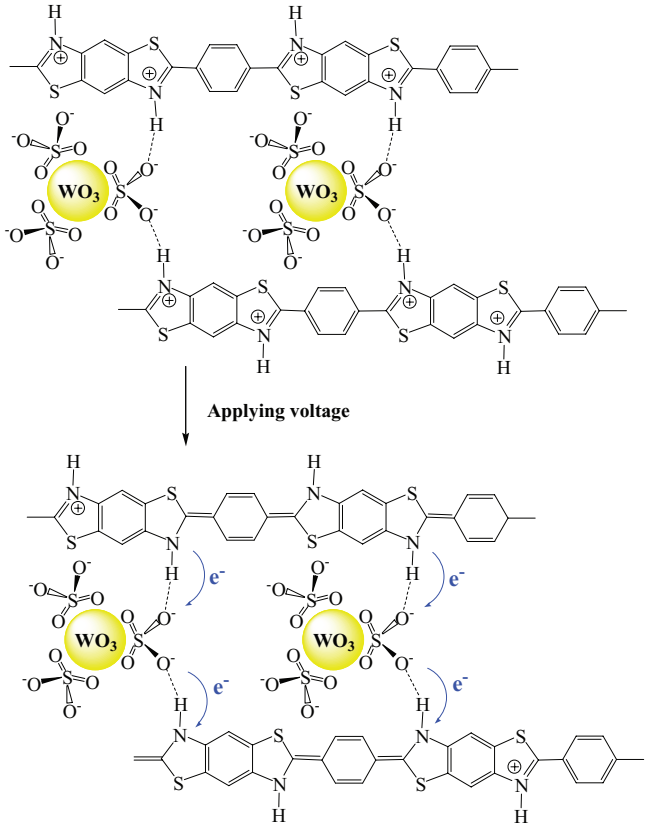

Figure 7. Scheme of PBZT structural transformation and interchain electron transfer after applying voltage (the drawing is not to scale).

For example, the background with "LAMAR" can be clearly recognized. The stable switch between these two states can be easily controlled by applying a low voltage, which is an essentially important characteristic for the applications of smart windows, displays and optical shutters. Normally, a sandwich structure of the electrochromic devices is often used, which consists of transparent electrodes, electrochromic material and solid (gel) electrolyte layer.[39–42] The thickness of the layers between the electrodes is controlled at micrometers to facilitate the electron transport through the electrochromic layer and to achieve highly efficient coloration. In this work, the full coloration of the PBZT thin film can be achieved even when the distance between the electrodes is ~25 mm without any electrolyte. Higher coloration efficiency and switching speed are expected when this material is designed in a sandwich structure.

Both the neutral and the reduced states of the pristine PBZT and WO_3/PBZT nanocomposite thin films are characterized by

Figure 8. The color change of the PBZT thin film before (A) and after (B) applying a voltage.

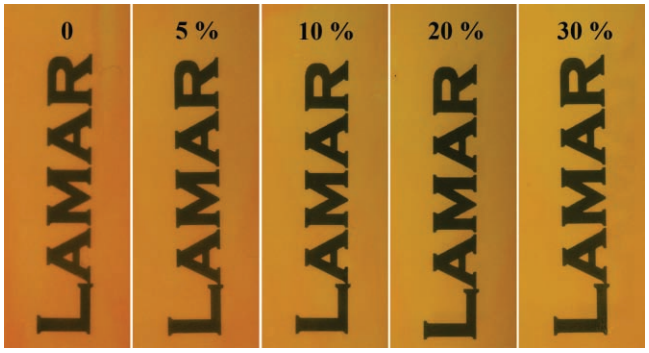

Figure 9. The transparency of the PBZT and WO_3/PBZT nanocomposite thin films casted from CSA solutions (the value at the top image indicates the weight percentage of the nano-WO_3 in the film).

UV-Vis spectroscopy. No peak shift is observed for the nanocomposite thin films in both neutral and reduced states as compared to that of the pristine PBZT thin film (Figure 4). This observation indicates that the planarity of the pristine PBZT and nanocomposite thin films is similar when they are protonated. Similar results are reported on the protonated conjugated polymers with different repeating units.[43] Identical absorption peaks are found at 470 and 506 nm in the neutral state, which are strongly red-shifted (compared with Figure 6) due to the protonated backbone structure of PBZT. Two new peaks at 464 and 639 nm are observed corresponding to the dark blue for the reduced state of PBZT (Figure 8B). However, the two original peaks disappear corresponding to orange, the color of pristine PBZT (Figure 8A). These results further prove the structural transformation of PBZT (Figure 7).

2.4. Transparency, Morphology, and Elemental Analysis

Figure 9 shows the pictures of the pristine PBZT and WO_3/PBZT nanocomposite thin films. The thin films are casted on the glass slides and covered on the paper where the word "LAMAR" is printed. The transparency of the thin films is well maintained after the addition of the nanoparticles, even in the WO_3/PBZT nanocomposite thin films with high particle loadings. Interestingly, the transparency is ever better when the particle loading increases to 30 wt%, and a slightly color change from orange to yellow is observed with the increase of the nanoparticle loading. In addition, the homogeneous color of the thin films indicates the uniform dispersion of the nanoparticles within the polymer matrix and high quality of the films.

Figure 10 shows the SEM microstructures of the pristine PBZT and WO_3/PBZT nanocomposite thin films with a nanoparticle loading of 5 wt%. The surface of nanocomposite thin film (Figure 10b) is much rougher, but still uniform as compared to that of the pristine PBZT (Figure 10a). The WO_3 nanoparticles are observed to be fairly uniformly dispersed in the PBZT thin film, especially depicted in the image with higher magnification (Figure 10c). The observed larger particles are due to the partial agglomerated nanoparticles and further work needs be done for better particle dispersion. The energy dispersive X-ray analysis (EDAX) elemental analysis of the nanoparticles

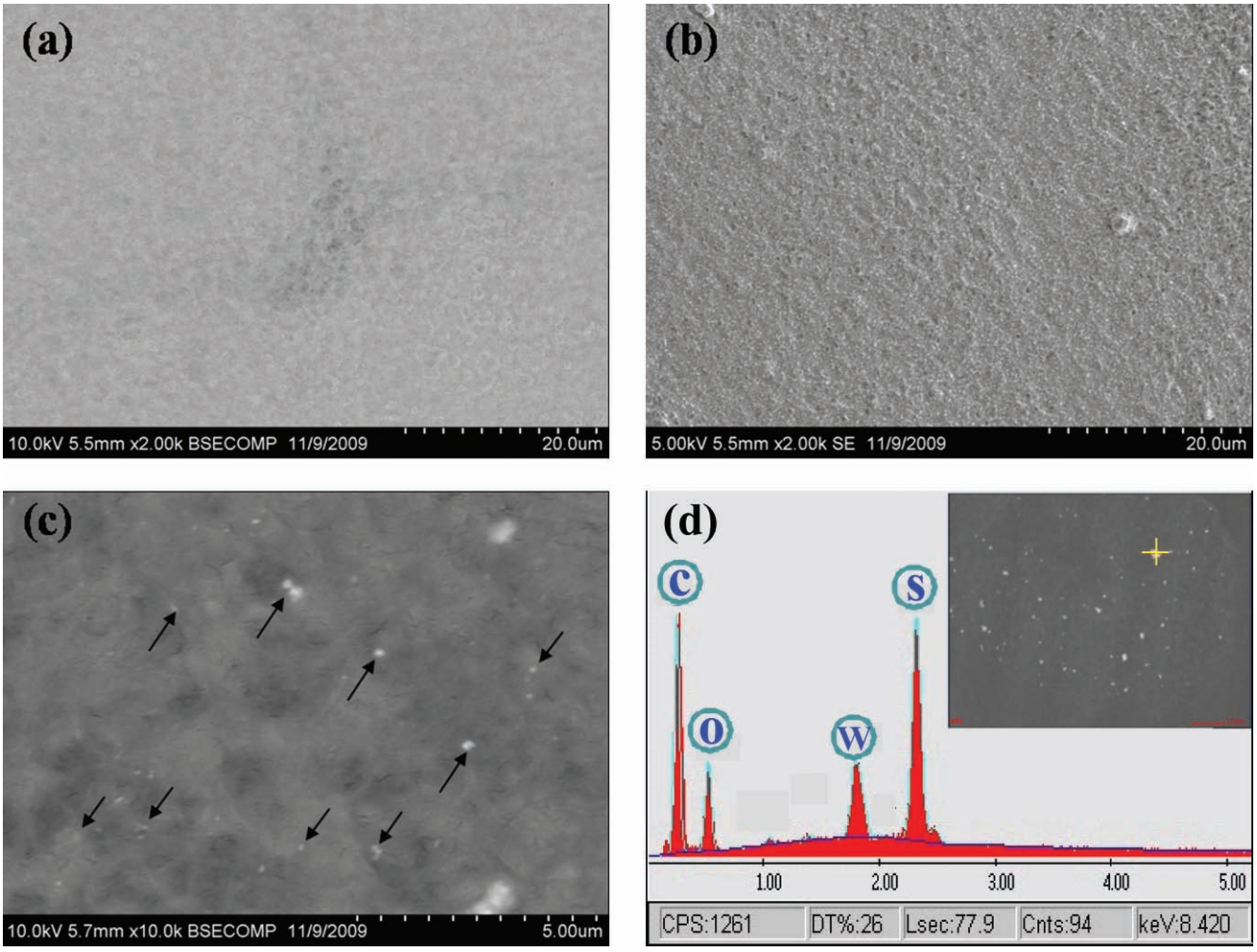

Figure 10. SEM microstructures of thin films of a) pristine PBZT, b) 5 wt% WO_3/PBZT (×2000), c) 5 wt% WO_3/PBZT (×10000), and d) EDAX spectrum obtained from the embedded particle (yellow cross).

embedded in the PBZT matrix reveals the presence of WO_3 nanoparticles even after the rigorous fabrication process (Figure 10d). In addition, strong sulfur peak is observed in the EDAX spectrum, indicating the strong absorption of sulfuric acid on the nanoparticle surface, which is in good agreement with the sulfuric acid assisted electron transport mechanism in Figure 7. The carbon element observed in the spectrum is from the substrate and the polymer.

3. Conclusion

Polymer nanocomposites comprising PBZT and WO_3 nanoparticles have been successfully fabricated with enhanced electrical switching and electrochromic properties in one step. CSA is chosen as solvent to dissolve PBZT and meanwhile it spontaneously transforms to the doping acid after exposing to air. Nanocomposites with lower nanoparticle loadings (5 wt%) show significant enhancement in electrical conductivity, which is about 200 times and 2 times, respectively, as compared to that of the as-received PBZT and PBZT/CSA thin films within the scanning voltage range of –1.0 V ~ –0.5 V. However, nanocomposites with higher loadings (20 wt% and 30 wt%) show ohmic conduction mechanism within the whole voltage of –1~1 V. SEM microstructure observation and EDAX elemental analysis reveal that the WO_3 nanoparticles are fairly uniformly dispersed in the polymer matrix. Stable electrical conductivity switching is also observed before and after applying bias on the pristine

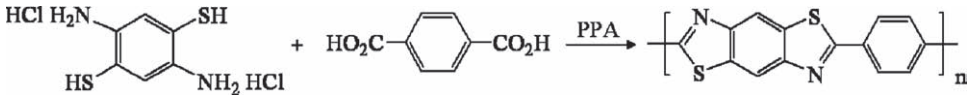

Scheme 2. Synthesis of PBZT.

PBZT and WO_3/PBZT nanocomposite films. Electrochromic phenomenon of both pristine PBZT and WO_3/PBZT nanocomposite thin films with high contrast ratio is observed after applying a small bias (3 V). The mechanisms of the nanoparticle in enhancing the electrical switching and electrochromic properties are explained in terms of creating a more efficient polymer intra-chain electron transfer pathway, which increases the electrical property.

4. Experimental Section

Materials: PBZT thin films (6 ~ 8 μm) are provided by the Air Force Research Laboratory and are dried at 80 °C in a vacuum oven for 24 h before use. PBZT are prepared by condensing 2,5-diamino-1,4-benzenediol dihydrochloride with terephthalic acid (**Scheme 2**).[8] Polyphospholic acid (PPA) is used as a solvent for the polycondensation reaction. CSA (97%) is purchased from Acros Organics. The WO_3 powers with an average diameter of 30 nm are obtained from Nanostructured & Amorphous Materials, Inc. All the materials are used as received without any further treatment.

Preparation of WO_3/PBZT Nanocomposite Thin Films: The WO_3/PBZT nanocomposites are prepared by the solution blending method. PBZT is first dissolved into CSA (w/w: 1/1000) with sonication for 0.5 h. Different weight fractions of WO_3 nanoparticles (5 wt%, 10 wt%, 20 wt% and 30 wt%) are mixed with the PBZT/CSA solution in a sealed vial with the aid of sonicator for 1 h. The WO_3/PBZT nanocomposite thin films are fabricated by dip-coating method, the same volume of the solutions are dropped on the glass slides to allow the same thickness of the WO_3/PBZT thin films. To test the electrochromic performance of the resulting thin films, two pieces of carbon fiber paper (CFP) (20 mm × 5 mm × 0.26 mm, Fuel Cell Store Inc.) are placed on the thin films at a fixed distance of 25 mm. The external voltage is supplied through the connection between the alligators and CFP. The CFP is used for two purposes: one is to enhance the electron transfer; the other is to avoid the direct contact of the metal alligator to thin film, since from our previous work,[28] metal will dope the thin film and make the color change.

Characterizations: The morphology of the pristine PBZT and WO_3/PBZT nanocomposites are evaluated using scanning electron microscopy (Hitachi S-3400 SEM). The EDAX attached to the SEM is used to characterize the elemental component of WO_3/PBZT nanocomposites. Fourier transform infrared spectroscopy (FT-IR, a Bruker Inc. Tensor 27 FT-IR spectrometer with hyperion 1000 ATR microscopy accessory) is used to characterize the pristine PBZT and WO_3/PBZT nanocomposite thin films. An ultraviolet visible spectrophotometer (UV-Vis, Cary 50) scanning from 800 nm to 200 nm is used to characterize the electrochromic properties of the nanocomposites. The electrical conductivity is measured by a standard four-probe technique (C4S 4-Point Probe Head, Cascade Microtech. Tips are made of tungsten carbide). To make sure that a precise voltage is applied on the two inner probes, V-source testing mode (Keithley 2400 source meter, USA) is introduced. The measured voltage is adjusted in the range of −1 V to 1 V and the corresponding current is measured and recorded across the two outer probes. Dimensions of the film used are 80 mm × 20 mm × (0.006 ~ 0.008) mm. External voltages (bias) are applied (3, 5, and 10 V) on the surfaces of the pristine PBZT and WO_3/PBZT nanocomposite thin films by a DC power unit (TEKPOWER HY1803D). However, applying different voltages does not show significant difference in the electrical conductivity, thus the smaller voltage (3 V) is used in this work. To avoid natural doping of copper wire, carbon fiber (CF) rod is used as electrodes and the distance between the two carbon fiber electrodes is adjusted about 25 mm. Four-point measurement is conducted for both situations when the external voltage is on and off. The detailed calculation of electrical conductivity is described in our previous work.[31]

Acknowledgements

This work was supported by the research start-up fund and research enhancement grant (REG) from Lamar University. The authors are grateful for the support of a NSF 2006 MRI Grant (Award No. 0618924) for SEM/EDS for carrying out the study.

Received: February 8, 2010
Revised: April 12, 2010
Published online: August 4, 2010

[1] K. M. Coakley, M. D. McGehee, *Chem. Mater.* **2004**, *16*, 4533.
[2] A. A. Argun, P.-H. Aubert, B. C. Thompson, I. Schwendeman, C. L. Gaupp, J. Hwang, N. J. Pinto, D. B. Tanner, A. G. MacDiarmid, J. R. Reynolds, *Chem. Mater.* **2004**, *16*, 4401.
[3] A. P. Kulkarni, C. J. Tonzola, A. Babel, S. A. Jenekhe, *Chem. Mater.* **2004**, *16*, 4556.
[4] B. Liu, G. C. Bazan, *Chem. Mater.* **2004**, *16*, 4467.
[5] R. J. Mortimer, *Electrochim. Acta* **1999**, *44*, 2971.
[6] J. Roncali, *Chem. Rev.* **1997**, *97*, 173.
[7] P. Mansky, T. P. Russell, C. J. Hawker, J. Mays, D. C. Cook, S. K. Satija, *Phys. Rev. Lett.* **1997**, *79*, 237.
[8] X.-D. Hu, S. E. Jenkins, B. G. Min, M. B. Polk, S. Kumar, *Macromol. Mater. Eng.* **2003**, *288*, 823.
[9] D. L. Meeker, D. S. K. Mudigonda, J. M. Osborn, D. C. Loveday, J. P. Ferraris, *Macromolecules* **1998**, *31*, 2943.
[10] J. L. Boehme, D. S. K. Mudigonda, J. P. Ferraris, *Chem. Mater.* **2001**, *13*, 4469.
[11] D. M. DeLongchamp, M. Kastantin, P. T. Hammond, *Chem. Mater.* **2003**, *15*, 1575.
[12] P. Mavinakuli, S. Wei, Q. Wang, A. B. Karki, S. Dhage, Z. Wang, D. P. Young, Z. Guo, *J. Phys. Chem. C* **2010**, *114*, 3874.
[13] S. Komaba, K. Fujihana, T. Osaka, *J. Electrochem. Soc.* **1998**, *145*, 1126.
[14] T. N. My, F. D. Arthur, *Adv. Mater.* **1994**, *6*, 858.
[15] Z. Guo, S. E. Lee, H. Kim, S. Park, H. T. Hahn, A. B. Karki, D. P. Young, *Acta Mater.* **2009**, *57*, 267.
[16] Z. Guo, S. Park, S. Wei, T. Pereira, M. Moldovan, A. B. Karki, D. P. Young, H. T. Hahn, *Nanotechnology* **2007**, *18*, 335704.
[17] R. J. Tseng, J. Huang, J. Ouyang, R. B. Kaner, Y. Yang, *Nano Lett.* **2005**, *5*, 1077.
[18] S. K. Pillalamarri, F. D. Blum, A. T. Tokuhiro, M. F. Bertino, *Chem. Mater.* **2005**, *17*, 5941.
[19] Y. Gao, D. Shan, F. Cao, J. Gong, X. Li, H.-y. Ma, Z.-m. Su, L.-y. Qu, *J. Phys. Chem. C* **2009**, *113*, 15175.
[20] M. M. Oliveira, E. G. Castro, C. D. Canestraro, D. Zanchet, D. Ugarte, L. S. Roman, A. J. G. Zarbin, *J. Phys. Chem. B* **2006**, *110*, 17063.
[21] D. Sun, H.-J. Sue, N. Miyatake, *J. Phys. Chem. C* **2008**, *112*, 16002.
[22] J. F. Wolfe, F. E. Arnold, *Macromolecules* **1981**, *14*, 909.
[23] J. F. Wolfe, B. H. Loo, F. E. Arnold, *Macromolecules* **1981**, *14*, 915.
[24] P. M. S. Monk, R. J. Mortimer, D. R. Rosseinsky, *Electrochromism: Fundamentals and Applications*, VCH, Weinheim **1995**.
[25] C. G. Granqvist, *Handbook of Inorganic Electrochromic Materials*, Elsevier, Amsterdam, **1995**.
[26] C. L. Gaupp, D. M. Welsh, R. D. Rauh, J. R. Reynolds, *Chem. Mater.* **2002**, *14*, 3964.
[27] M. Li, Y. Sheynin, A. Patra, M. Bendikov, *Chem. Mater.* **2009**, *21*, 2482.
[28] M.-A. De Paoli, A. Zanelli, M. Mastragostino, A. M. Rocco, *J. Electroanal. Chem.* **1997**, *435*, 217.
[29] P. Jia, A. A. Argun, J. Xu, S. Xiong, J. Ma, P. T. Hammond, X. Lu, *Chem. Mater.* **2009**, *21*, 4434.
[30] D. Y. Shen, S. L. Hsu, *Polymer* **1982**, *23*, 969.

[31] J. Zhu, S. Wei, M. Jr. Alexander, D. Cocke, T. C. Ho, Z. Guo, *J. Mater. Chem.* **2010**, *20*, 568.
[32] J. E. Yoo, W. P. Krekelberg, Y. Sun, J. D. Tarver, T. M. Truskett, Y.-L. Loo, *Chem. Mater.* **2009**, *21*, 1948.
[33] F. Chen, J. He, C. Nuckolls, T. Roberts, J. E. Klare, S. Lindsay, *Nano Lett.* **2005**, *5*, 503.
[34] P. G. Pickup, W. Kutner, C. R. Leidner, R. W. Murray, *J. Am. Chem. Soc.* **1984**, *106*, 1991.
[35] W. Lu, A. G. Fadeev, B. Qi, E. Smela, B. R. Mattes, J. Ding, G. M. Spinks, J. Mazurkiewicz, D. Zhou, G. G. Wallace, D. R. MacFarlane, S. A. Forsyth, M. Forsyth, *Science* **2002**, *297*, 983.
[36] M. Mitsuyuki, *J. Polym. Sci., Part B: Polym. Phys.* **1994**, *32*, 231.
[37] M. F. Roberts, S. A. Jenekhe, *Chem. Mater.* **1993**, *5*, 1744.
[38] M. F. Roberts, S. A. Jenekhe, A. Cameron, M. McMillan, J. Perlstein, *Chem. Mater.* **1994**, *6*, 658.
[39] C. A. Nguyen, S. Xiong, J. Ma, X. Lu, P. S. Lee, *J. Phys. Chem. B* **2009**, *113*, 8006.
[40] I. Schwendeman, R. Hickman, G. Sonmez, P. Schottland, K. Zong, D. M. Welsh, J. R. Reynolds, *Chem. Mater.* **2002**, *14*, 3118.
[41] C. Marcel, J. M. Tarascon, *Solid State Ionics* **2001**, *143*, 89.
[42] D. DeLongchamp, P. T. Hammond, *Adv. Mater.* **2001**, *13*, 1455.
[43] J. A. Osaheni, S. A. Jenekhe, *Chem. Mater.* **1995**, *7*, 672.